JOURNAL OF ENVIRONMENTAL SCIENCES 96 (2020) 186–193

Available online at www.sciencedirect.com

ScienceDirect

www.elsevier.com/locate/jes

JES JOURNAL OF ENVIRONMENTAL SCIENCES

www.jesc.ac.cn

Arsenic and cadmium removal from water by a calcium-modified and starch-stabilized ferromanganese binary oxide

Huxing Chen[1], *Fangnan Xu*[1], *Zhengzheng Chen*[2], *Ouyuan Jiang*[2], *Williamson Gustave*[3], *Xianjin Tang*[2,*]

[1] *School of Materials Science and Engineering, Zhejiang University, Hangzhou 310027, China*
[2] *Institute of Soil and Water Resources and Environmental Science, Zhejiang Provincial Key Laboratory of Agricultural Resources and Environment, Zhejiang University, Hangzhou 310058, China*
[3] *School of Chemistry, Environmental & Life Sciences, University of The Bahamas, New Providence, Nassau, The Bahamas*

ARTICLE INFO

Article history:
Received 25 December 2019
Revised 1 March 2020
Accepted 2 March 2020
Available online 30 May 2020

Keywords:
Arsenic
Cadmium
Calcium
Fe–Mn binary oxide
Complexation
Adsorption

ABSTRACT

A new calcium-modified and starch-stabilized ferromanganese binary oxide (Ca-SFMBO) sorbent was fabricated with different Ca concentrations for the adsorption of arsenic (As) and cadmium (Cd) in water. The maximum As(III) and Cd(II) adsorption capacities of 1% Ca-SFMBO were 156.25 mg/g and 107.53 mg/g respectively in single-adsorption systems. The adsorption of As and Cd by the Ca-SFMBO sorbent was pH-dependent at values from 1 to 7, with an optimal adsorption pH of 6. In the dual-adsorbate system, the presence of Cd(II) at low concentrations enhanced As(III) adsorption by 33.3%, while the adsorption of As(III) was inhibited with the increase of Cd(II) concentration. Moreover, the addition of As(III) increased the adsorption capacity for Cd(II) up to two-fold. Through analysis by X-ray photoelectron spectroscopy (XPS) and Fourier-transform infrared spectroscopy (FTIR), it was inferred that the mechanism for the co-adsorption of Cd(II) and As(III) included both competitive and synergistic effects, which resulted from the formation of ternary complexes. The results indicate that the Ca-SFMBO material developed here could be used for the simultaneous removal of As(III) and Cd(II) from contaminated water.

Introduction

Waterbodies contaminated with toxic trace elements are a widespread problem, especially in developing countries (Agrafioti et al., 2014). These waterbodies may become contaminated with heavy metal(loid)s from both point-source and non-point-source pollutants. Heavy metal(loid) ions such as arsenic (As) and cadmium (Cd) in the waterbodies are potential ecological threats because these toxins can enter the food chain through drinking and irrigation water systems (Fisher et al., 2017; Ma et al., 2012; Zhao et al., 2019). Studies have shown that As and Cd can accumulate in living organisms, and cause a variety of harmful effects (Yan et al., 2015). As an illustration, both As and Cd have been observed to cause cancer and organ failure in humans (Barrett, 2012; Lubin et al., 2008). Therefore, there is an urgent need for the elimination of these elements. Previous studies have employed many methods such ion-exchange, electrochemical techniques, membrane filtration and reverse osmosis (Sullivan et al., 2010; Zhang et al., 2010). However, the use of these techniques for the removal of As and Cd from large waterbodies can be technically challenging and exorbitant in cost (De Gisi et al., 2016;

* Corresponding author:
E-mail: xianjin@zju.edu.cn (X. Tang).

https://doi.org/10.1016/j.jes.2020.03.060
1001-0742/

Ungureanu et al., 2015). Thus, it is of high importance to develop effective technologies that are cost-effective to treat As and Cd in large waterbodies before releasing them into the natural environment.

The advantage of using relatively easy-to-manufacture and cost-effective materials make adsorption methods popular in the treatment of large contaminated waterbodies (Deng et al., 2013). Previous investigations have used both chemical and biological absorbents, such as zeolites, clays, biochar and bacterium cells for the adsorption of As and Cd (Kyzas and Matis, 2015; Pandey et al., 2009; Wang and Xing, 2004). However, these absorbents do not have high removal efficiencies (Han et al., 2013; Mishra and Ramaprabhu, 2010). Previous studies on As (III) have shown that absorbents combined with ferromanganese binary oxide (FMBO) could improve the removal efficiency of As(III) from water (Gallios et al., 2017; Lou et al., 2017). This is due to the fact that FMBO has a porous structure with large specific surface area, and contains Mn and Fe functional groups (McCann et al., 2018; Wu et al., 2015). The improved adsorption of As(III) by FMBO was due to the oxidation of As(III) to As(V) by Mn(V) (Xu et al., 2019). Furthermore, the Fe(III) oxide component can serve as an adsorption site for As(III) and As(V) and facilitate As removal from the water (Ryu et al., 2017).

Although Fe–Mn binary oxides are efficient in removing As(III) from aqueous solutions, they are less effective in absorbing Cd. Since Cd exists as a cation in solution and tend not to precipitate with Fe(III) oxide, as is observed with As(V) and Fe oxides. Thus, it is difficult to simultaneously remove As and Cd by FMBO alone. In a previous study on municipal solid wastes, an increase of Ca content positively contributed to the stabilization of heavy metal cations (Agrafioti et al., 2014). Thus, in this study, based on the above information, we added $CaCO_3$ on the surface of starch-FMBO (Xu et al., 2019) in an attempt to improve its Cd absorption capacity. Furthermore, an adsorption experiment was carried out to determine the optimum Ca content and pH conditions for the removal of As and Cd. The adsorption performance of Ca-SFMBO for As and Cd in water was studied by a thermodynamic adsorption experiment. Further, X-ray diffraction (XRD), scanning electron microscopy equipped with energy dispersive spectroscopy (SEM-EDS), X-ray photoelectron spectroscopy (XPS), and Fourier-transform infrared spectroscopy (FT-IR) were used to study the absorption mechanism.

1. Materials and methods

1.1. Materials

Analytical grade chemical reagents including $FeSO_4{\cdot}7H_2O$, $Fe_2(SO_4)_3$, $MnSO_4$, $KMnO_4$, $CaCO_3$, NaOH, and HCl were obtained from the Sinopharm Chemical Reagent Co., Ltd., China. The stock solutions of As(III) (300 mg/L) and Cd(II) (300 mg/L) were prepared by dissolving $NaAsO_2$ and $Cd(NO_3)_2$ (Analytical Reagent) in deionized water, respectively.

1.2. Synthesis of adsorbents

Ca-SFMBO was synthesized by using a co-precipitation method in the presence of a stabilizer (starch) and surface modifier ($CaCO_3$). Firstly, a 0.0412 g/mL stock solution of starch and a mixture of $FeSO_4{\cdot}7H_2O$ (0.1860 g/mL) and $MnSO_4$ (0.0100 g/mL) were prepared in deionized water. Secondly, 10 mL of the prepared solution was mixed with 30 mL of iron manganese solution in a 100 mL beaker for 15 min. Then, 25 mL $KMnO_4$ (0.0504 g/mL) was gradually added to the mixture and stirred vigorously with a magnetic stirrer. After mixing completely, 4 mol/L NaOH was used the adjust the pH of the mixture to 2. The solution was allowed to equilibrate for 24 hr at 25 °C before the suspension was filtered using 30–50 μm filter paper and washed with deionized water three times. The starch-stabilized iron manganese oxide (SFMBO) product was thus obtained. Finally, SFMBO was uniformly dispersed into deionized water to form a turbid liquid. Calcium carbonate powder with different mass fractions (0%, 1%, 5% and 10%) was added into the turbid suspension of SFMBO and the mixture was dispersed by ultrasound for 1 hr. The mixture was then separated by suction filtration, washed with deionized water three times, and dried for 24 hr.

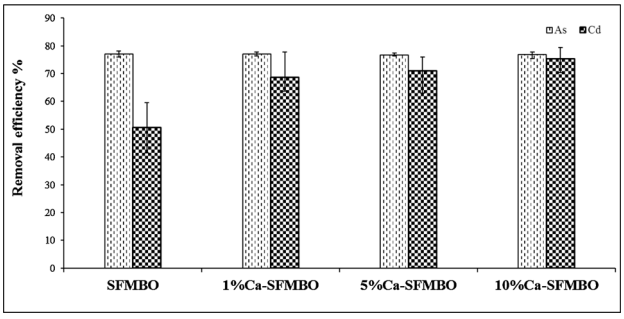

Fig. 1 – Effect of Ca-SFMBO concentration on the removal efficiency (%) of Cd(II) and As(III) after a 24 hr. incubation period in single-adsorbate systems. The initial concentration of As(III) was 30 mg/L and initial concentration of Cd(II) was 20 mg/L at pH 5. SFMBO: starch-stabilized ferromanganese binary oxide; Ca-SFMBO: calcium-modified and starch-stabilized ferromanganese binary oxide.

$CaCO_3$ particles were added to the freshly prepared SFMBO and sonicated to adjust the SFMBO surface chemistry (Gurgel et al., 2008) through reaction of Ca^{2+} with ferric and manganese oxides (Wu et al., 2018). The addition of $CaCO_3$ decreased the acidity of the SFMBO surface environment and enhanced the activity of Fe and Mn oxide adsorption sites, which can contribute to the direct adsorption of Cd(II) (Sheng et al., 2004).

1.3. Characterization

The surface morphology and particle size of the material were detected by scanning electron microscopy (SEM, FEI-Quanta 200F, FEI, Netherlands), and the distribution and content of elements could be qualitatively analyzed by energy dispersive spectroscopy (EDS, SIRON, FEI, Netherlands). X-ray diffraction (XRD, XD-98, Netherlands) was used to detect the crystal structures of materials. In addition, the influence of functional groups on the material surface and the adsorption mechanism before and after the adsorption of As and Cd were investigated by X-ray photoelectron spectroscopy (XPS, Escalab 250 xi, Thermo Fisher Scientific, USA) and Fourier-transform infrared spectroscopy (FT-IR, IRaffinity-1, SHIMADZU, Japan).

1.4. Batch experiments

Batch thermodynamic adsorption experiments were carried out to evaluate the adsorption capacities of the adsorbents for As(III) and Cd(II). All deionized water used in the adsorption experiment was purged with nitrogen for 10 min in advance to remove all oxygen from the water. In detail, 0.0100 g of adsorbent was added into a 50 mL centrifuge tube, and the adsorption capacity for different concentrations of As(III) and Cd(II) (0–70 mg/L) was evaluated. The adsorption capacity of the adsorbents in an As(III)-Cd(II) mixed solution was also tested.

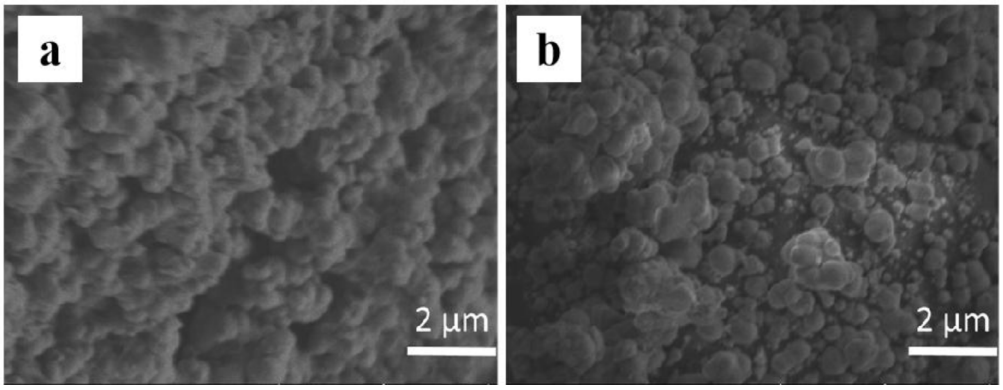

Fig. 2 – SEM images of different adsorbents: (a) SFMBO; (b) 1%Ca-SFMBO.

The effect of adsorption pH (As(III) solution in the range 1–11, Cd(II) solution in the range 1–7 and dual-adsorbate system in the range 1–7) on adsorption was also studied. The tubes were placed in a thermostatic oscillator (250 r/min, 25 °C) for 24 hr., and the suspension was filtered using a 0.45-μm hydrophilic membrane after 24 hr. Then, the concentrations of total As(III) and Cd(II) were analyzed by Inductively Coupled Plasma Mass Spectrometry (ICP-MS NEXION300XX, PerkinElmer, Inc., USA).

2. Results and discussion

2.1. *Selection and characterization of Ca-SFMBO*

Fig. 1 shows the removal efficiency of SFMBO for As(III) and Cd(II). The removal efficiency toward As(III) was 77.1%, while that for Cd(II) was 50.6%. In order to improve the removal efficiency toward Cd (II), the surface of SFMBO was modified with $CaCO_3$ powder. The addition of $CaCO_3$ (1% mass fraction) greatly improved the removal efficiency for Cd(II) (68.7%), but only had minimal influence on the As(III) removal efficiency. It has been reported that increasing amounts of calcium carbonate increased the pH by three units on the surface of biochar Wu et al., 2018); further, Guan et al. (2017) confirmed that $CaCO_3$-modified diatomite could improve its treatment efficiency in acid dye wastewater. Besides, Chun et al. (2004) also modified the surface of HZSM-5 zeolite by $CaCO_3$ through a solid-state reaction, and indicated that the acidity of the samples was reduced after modification. The mechanism is similar to Reaction ((1) (Xu et al., 2014).

$$\mathrm{SFMBO-a(H^+)+bCaCO_3 \rightarrow SFMBO-c(Ca)+dHCO_3^- + eH_2CO_3} \quad (1)$$

However, further increasing the dosage of $CaCO_3$, to as high as 10% mass fraction, did not significantly improve the removal efficiency toward both As(III) and Cd(II). This may have occurred because further increasing the $CaCO_3$ content had little impact on the surface pH of SFMBO. Moreover, high-concentration $CaCO_3$ could reduce the active iron oxide and manganese oxide components of SFMBO as follows:

$$\mathrm{SFMBO-f(OH)+gCaCO_3 \rightarrow SFMBO-h(OCa^+)+iHCO_3^- + jH_2CO_3} \quad (2)$$

and this could also influence the heavy metal(loid) adsorption kinetics (Zhang et al., 2009b).

There were no detectable crystalline peaks in the XRD patterns of SFMBO and Ca-SFMBO (1%-10% Ca), indicating that SFMBO was amorphous and had interior porosity (not shown in this paper) (Shan and Tong, 2013). As shown in Fig. 2, the surface morphology of SFMBO and Ca-SFMBO is composed of loose particles, and the distribution of SFMBO particles (100–200 nm) was relatively uniform. The size of Ca-SFMBO particles was as small as a few tens of nanometers and as large as 500 nm, which was not uniform. This occurred because when adding the $CaCO_3$ modifier, the acid-base balance on the surface of SFMBO was destroyed and became more basic, which promoted the aggregation and growth of iron- and manganese- oxide particles (Ebinger and Schulze, 1990; Gu et al., 2017).

2.2. *Optimization of initial pH for As/Cd adsorption by Ca-SFMBO in water*

The influence of the initial pH on the As(III) adsorption capacity is shown in Fig. 3a. Ca-SFMBO could maintain a stable adsorption capacity for As(III) over a wide pH range, and the adsorption effect was best when the pH was 10. This occurred because during the synthesis of the adsorbent (pH = 2), the pH was tightly controlled, resulting in an increase in proton functional groups on the surface of Ca-SFMBO. Since, in an alkaline environment, a proton protective layer was formed on the surface of the adsorbent to prevent passivation of iron and manganese ions; this consequently facilitated As(III) oxidation by MnO_2 to As(V), which enhanced As adsorption in the form of $H_2AsO_4^-$, $HAsO_4^{2-}$, and AsO_4^{3-} (Lin et al., 2017; Xiong et al., 2017). When the pH reached 11, the protective proton layer on the surface of the adsorbent was destroyed. In the higher pH range, the adsorption of As(III) was inhibited by the negatively charged sites occupying the surface of the material and the electrostatic repulsion effect (Yang et al., 2010), resulting in a decrease in the removal efficiency of As(III).

Cd(II) is unstable under alkaline conditions and is prone to the formation of cadmium hydroxide, which inhibits the normal adsorption of Cd(II) (Reddy and Lee, 2014). Therefore, the initial pH in Cd(II) adsorption experiments ranged from 1 to 7 (Fig. 3b). The adsorption of Cd(II) by Ca-SFMBO was due to specific adsorption and physical adsorption by iron and manganese oxides. With the increase of initial pH, the proton layer on the surface of Ca-SFMBO was gradually removed, which resulted in the increase of specific adsorption sites for Cd(II) on the Ca-SFMBO surface and the adsorption capacity of Cd(II) (Roonasi and Holmgren, 2009). However, with the increase of pH, the hydroxyl groups in the solution combined with a large amount of iron and manganese ions to cause steric hindrance, hindering the specific adsorption sites of Cd(II), and inhibiting the adsorption of Cd(II).

The changes in the adsorption mode of Cd(II) in the As(III)-Cd(II) mixed contaminant solution are shown in Fig. 3c. In ad-

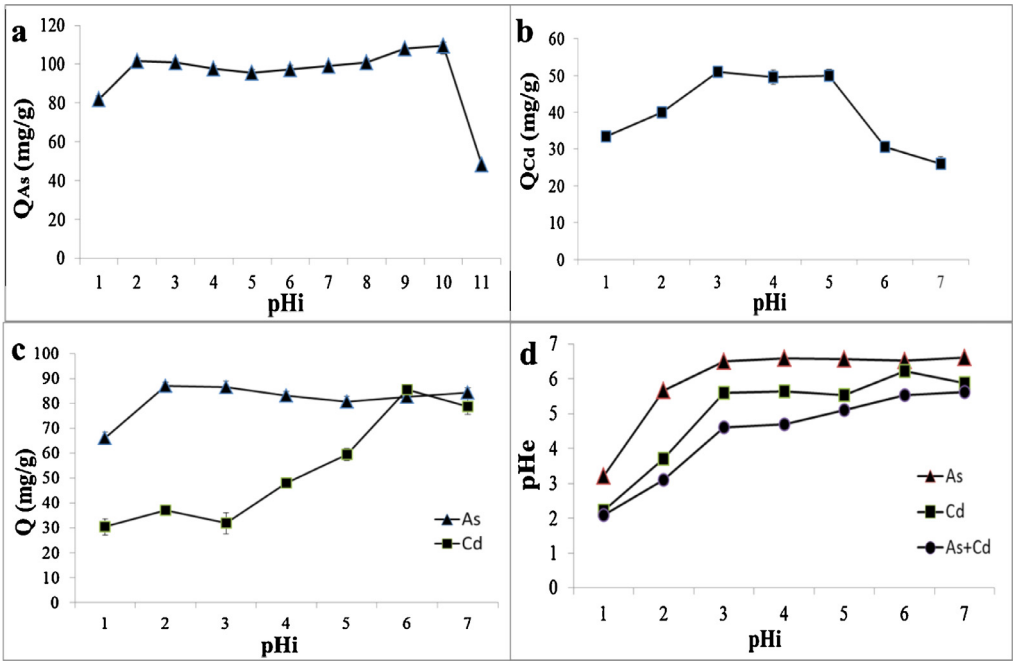

Fig. 3 – Effect of initial pH (pHi) on adsorption capacity of (a) As(III), (b) Cd(II), (c) As(III)-Cd(II), (d) equilibrium pH (pHe) at the initial As(III) concentration of 30 mg/L and initial Cd(II) concentration of 30 mg/L with equilibrium time of 24 hr. for As(III) and Cd(II).

Table 1 – The adsorption capacities of Fe-based adsorbents for As(III) and Cd(II) in water, from the literature.

No.	Adsorbent	Adsorption pH	Adsorption capacity (mg/g)		References
			As(III)	Cd(II)	
1	Calcium-based magnetic biochar (Ca-MBC)	6.0	6.34	10.07	Wu et al., 2018
2	Magnetic graphene oxide (MGO)	6.0	–	91.29	Deng et al., 2013
3	Fe/Mn modified biochar (FMBC)	7.0	8.25	–	Lin et al., 2017
4	Fe-Mn binary oxide nanohybrids	7.0	78.84	–	Lou et al., 2017
5	Fe-Mn binary oxide waste	7.0	70	–	McCann et al., 2018
6	Iron and manganese oxides	–	132	–	Ocinski et al., 2016
7	Fe-Mn binary oxide-impregnated granular activated carbon (IMIGAC)	7.5	18.4	–	Ryu et al., 2017
8	Magnetic nanoparticles modified with Fe-Mn binary oxide (Mag-Fe-Mn)	7.0	47.76	–	Shan and Tong, 2013
9	Iron hydroxide/manganese dioxide doped straw activated carbon	3.0	75.82	–	Xiong et al., 2017
10	Fe-Mn binary oxide	8.0	–	41.44	Xu et al., 2014
11	FeOOH	8.0	–	12.32	Xu et al., 2104
12	$MnFe_2O4$	3.0	94	–	Zhang et al., 2010
13	calcium-modified and starch stabilized ferromanganese binary oxide (Ca-SFMBO)	6.0	156.25	107.53	This study

dition to the original specific adsorption and physical adsorption modes, chemical complexation adsorption may have also played a role (Liu et al., 2015). As(III) was first oxidized to As(V) by manganese oxide, and then combined with the hydroxides of iron and manganese, making the previously positively charged surface of the adsorbents more negatively charged. This created a new adsorption site for Cd(II), through the formation of ternary complexes (Hu et al., 2015). The change in the initial pH had little effect on the adsorption capacity for As(III). However, compared with the monometallic As(III) system, the adsorption capacity significantly decreased, which was closely related to the presence of Cd(II). The adsorption capacity for Cd(II) greatly increased in the presence of As(III), and reached a stable value when the initial pH ranged from 6 to 7. Therefore, in the adsorption experiment of As(III)-Cd(II) mixed contaminant solutions, the initial pH was set at 6.

From the pH equilibrium curves (Fig. 3d), it can be observed that, after application of Ca-SFMBO, both the As and the Cd solutions maintained a stable pH (5–6) after equilibrium. The pH remained stable after the initial equilibrium, because the Ca-SFMBO adsorbent was fabricated under acidic conditions and this resulted in an increase of proton functional groups on the Ca-SFMBO surface. However, as the pH became more basic, a proton protective layer developed on the surface of the Ca-

SFMBO adsorbent and this prevented the iron and manganese ions from being passivated (Xu et al., 2019).

2.3. *Adsorption performance of Ca-SFMBO for As/Cd in water*

Adsorption equilibrium isotherm experiments for As(III) and Cd(II) were performed at pH 6 by varying the initial concentrations (As(III): 5–60 mg/L; Cd(II): 3–66 mg/L), and used to evaluate the As(III) and Cd(II) adsorption capacities of the adsorbents. The Langmuir equation is expressed as follows (Sun et al., 2018; Yang et al., 2006):

$$\frac{C_e}{Q_e} = \frac{1}{K_L Q_m} + \frac{C_e}{Q_m} \quad (3)$$

where Q_e (mg/g) and Q_m (mg/g) represent the equilibrium and the maximum adsorption capacity, respectively; C_e (mg/L) is the concentration of arsenic in the solution phase at equilibrium; K_L (L/mg) is the Langmuir adsorption equilibrium constant, which represents the affinity of arsenic adsorption.

The obtained isotherms are presented in Fig. 4a. According to the Langmuir equation, the calculated As(III) and Cd(II) adsorption capacities were 156.25 mg/g and 107.53 mg/g, respectively. Table 1 shows the adsorption capacities of As(III) and Cd(II) reported in other literatures. The correlation coefficients of both As(III) and Cd(II) could reach 0.99, indicating that the Langmuir model is suitable to describe the adsorption behavior of 1%Ca-SFMBO toward As(III) and Cd(II). The Langmuir adsorption equilibrium constant K_L of As(III) (0.32) is higher than that for Cd(II) (0.24), which means that As(III) is more easily adsorbed.

At different initial As(III) concentrations, the adsorption of As(III) varied with increasing amounts of Cd(II) (Fig. 4b). Addition of Cd(II) at about 3 to 9 mg/L could promote the adsorption of As(III), among which 3 mg/L Cd(II) had the greatest promoting effect on the absorption efficiency. When the added amount of Cd(II) was more than 17 mg/L, the presence of Cd(II) inhibited the adsorption of As(III). The presence of a small amount of Cd(II) could enhance the aggregation of $H_2AsO_4^-$, $HAsO_4^{2-}$, and AsO_4^{3-}, promoting the adsorption of anions from the solution on the adsorbent surface (Wu et al., 2018). However, in the co-adsorption system, competition for adsorption sites existed between As(III) and Cd(II) in most treatments because the surface adsorption sites of Ca-SFMBO were limited. Thus increasing the concentration of Cd(II) would occupy the adsorption sites for As(III) and As(V) and inhibit the adsorption process of As(III) (Han et al., 2015). Consequently, the adsorption of As(III) decreased successively in the solutions containing 17 mg/L, 33 mg/L and 66 mg/L of Cd(II).

At different initial Cd(II) concentrations, the adsorption capacity of Cd(II) gradually increased with the concentration of As(III) (Fig. 4c). When the initial concentration of Cd(II) was 33 mg/L, the adsorption capacity of Cd(II) in the 60 mg/L solution with As(III) content reached 113.9 mg/L, which was a great improvement compared with the adsorption capacity of Cd(II) (61.15 mg/L) without As(III) content.

If the adsorption mechanism in the co-adsorption system was only competitive adsorption, such as by specific adsorption and physical adsorption, the increase in the concentration of one ion would reduce the adsorption amount of the other ion (Wu et al., 2018). However, the data in Fig. 4c shows that another adsorption mechanism existed, chemical complexation adsorption. This might be explained by the following process (Liu et al., 2015): After the adsorption of some $H_2AsO_4^-$, $HAsO_4^{2-}$, AsO_4^{3-} on the surface of Ca-SFMBO, a new negative ion adsorption site was generated, and the Cd(II)

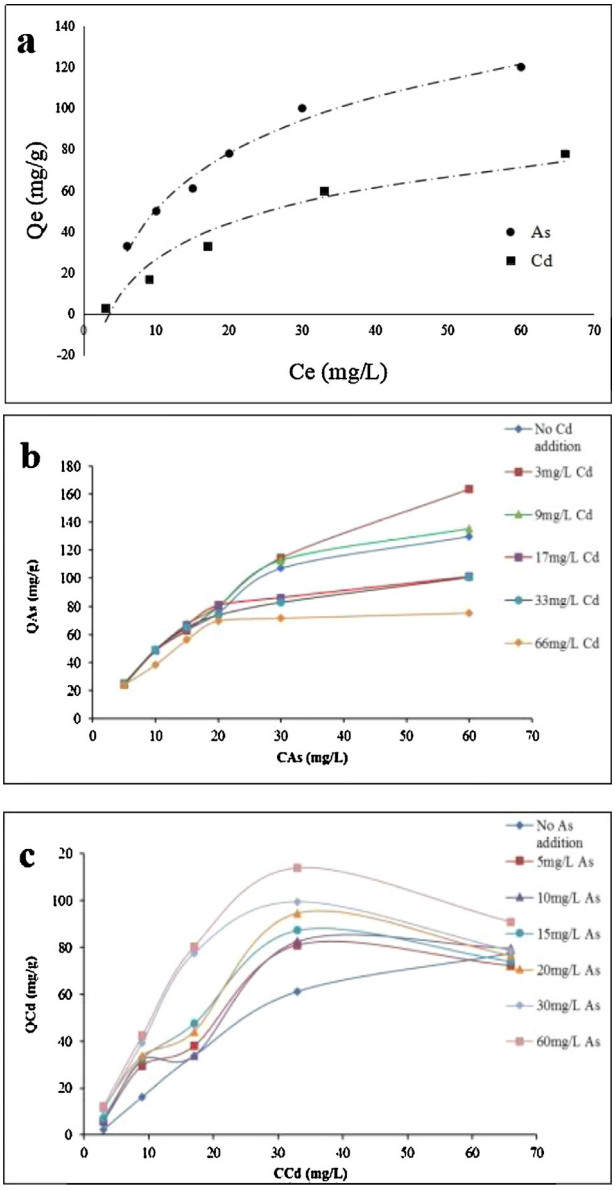

Fig. 4 – The effect of initial concentration (C_{As}, C_{Cd}) on adsorption capacity (Qe) of Cd(II) and As(III) in 1%Ca-SFMBO adsorbent experiments at initial pH 6. (a) shows the isotherms for As(III) and Cd(II) adsorption. (b) shows the effect of Cd(II) addition on As(III) adsorption. (c) shows the effect of As(III) addition on Cd(II) adsorption.

cation was attracted by electrostatic forces. Finally, a new stable chemical bond was formed at the adsorption site, forming a ternary complex. Therefore, the cationic adsorption sites on the surface of the original adsorbent were fully utilized, which greatly increased the adsorption capacity for Cd(II) (Hu et al., 2015).

According to the microscopic characterization analysis in Section 2.4, we inferred that the addition of As(III) in the solution promoted the formation of ternary complexes to promote the adsorption of Cd(II). In order to determine whether the ternary complex was type A (Fe-Cd-As) or type B (Fe-As-Cd), Wu et al. (2018) conducted experiments on the addition sequence of arsenic and cadmium. It was found that magnetic biochar (MBC), which was pretreated with saturated As

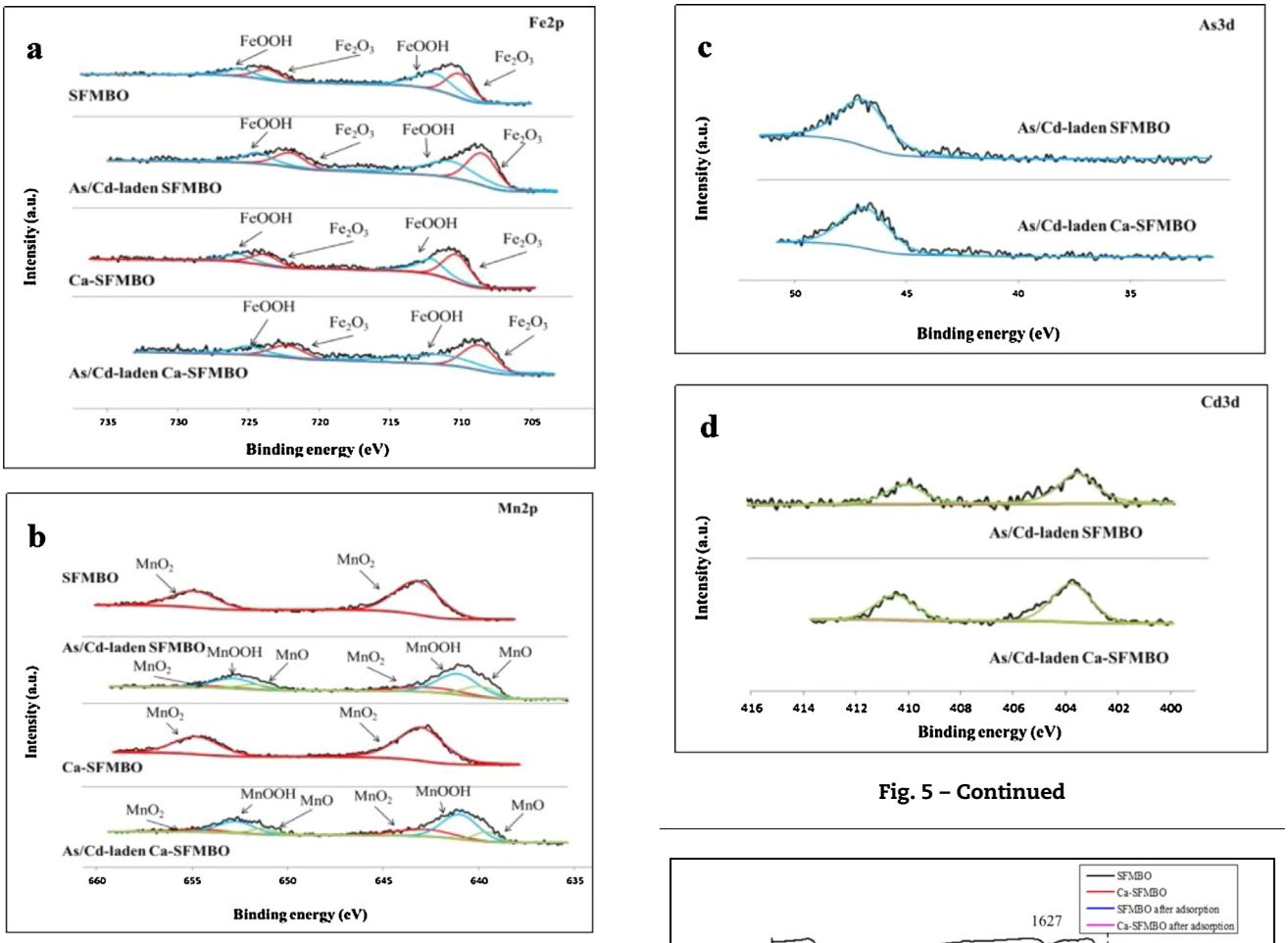

Fig. 5 – (a) Fe 2p; (b) Mn 2p; (c) As 3d and (d) Cd 3d narrow-scan XPS spectra of SFMBO, Ca-SFMBO, As/Cd-laden SFMBO, and As/Cd-laden Ca-SFMBO.

adsorption, significantly increased the adsorption capacity of Cd; however, when it was pretreated by saturated Cd adsorption, the adsorption capacity of the MBC for As was significantly decreased. This was because the MBC pretreated with saturated As adsorption produced new adsorption sites for Cd (MBC-As-), which improved the adsorption of Cd; while when it was pretreated with saturated Cd adsorption, Cd occupied a large number of As adsorption sites on the MBC, which decreased the adsorption capacity for As. Therefore, the ternary complex in the experiment is type B (Fe-As-Cd). In our study, the results also confirmed the existence of the type B ternary complex (as shown in Fig. 5), which is consistent with the results by Wu et al. (2018). However, more experiments with different As and Cd addition sequences should be conducted in the future.

2.4. *Adsorption mechanism*

XPS analysis of SFMBO and Ca-SFMBO adsorbents before and after the adsorption of As and Cd was conducted to study the adsorption mechanism. As shown in Fig. 5a, peaks were observed centered at 709.8 eV and 713.6 eV, indicating that the main forms of Fe(III) in the adsorbents were Fe_2O_3 and FeOOH (Cao et al., 2012). Calculation of the peak areas after As(III)-Cd(II) adsorption showed that the content of FeOOH decreased in both SFMBO and Ca-SFMBO, indicating that FeOOH

Fig. 5 – Continued

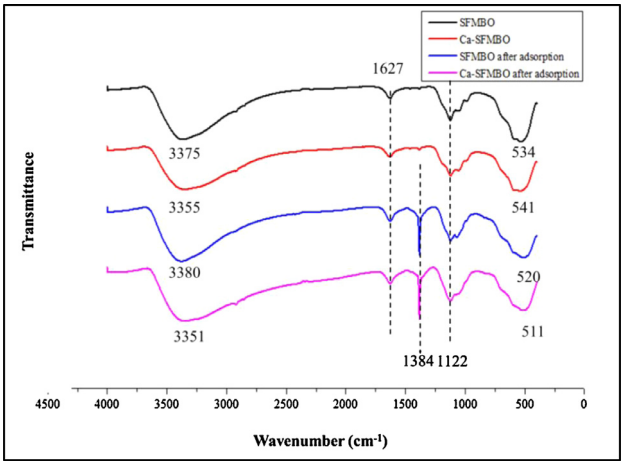

Fig. 6 – FT-IR spectra of SFMBO, and 1%Ca-SFMBO particles before and after As(III)-Cd(II) adsorption.

was consumed during the process. However, the valence state of Fe did not change with adsorption, suggesting that FeOOH was the adsorption component in the As(III)-Cd(II) adsorption process. Comparing spectra before and after adsorption, the peaks of FeOOH and Fe_2O_3 were shifted to higher binding energies, indicating that the formation of an adsorbed ternary complex in the form Fe-As-Cd changed the chemical state of Fe in the adsorbents (Xiong et al., 2017).

MnO_2 was the main form of Mn in the adsorbents, whose main function was to oxidize As(III). When As(III) was oxidized to As(V), the form of As in solution changed from H_3AsO_3 to $H_2AsO_4^-$, $HAsO_4^{2-}$ and AsO_4^{3-}, with a negative charge, which was more easily absorbed by cations on the surface of the ad-

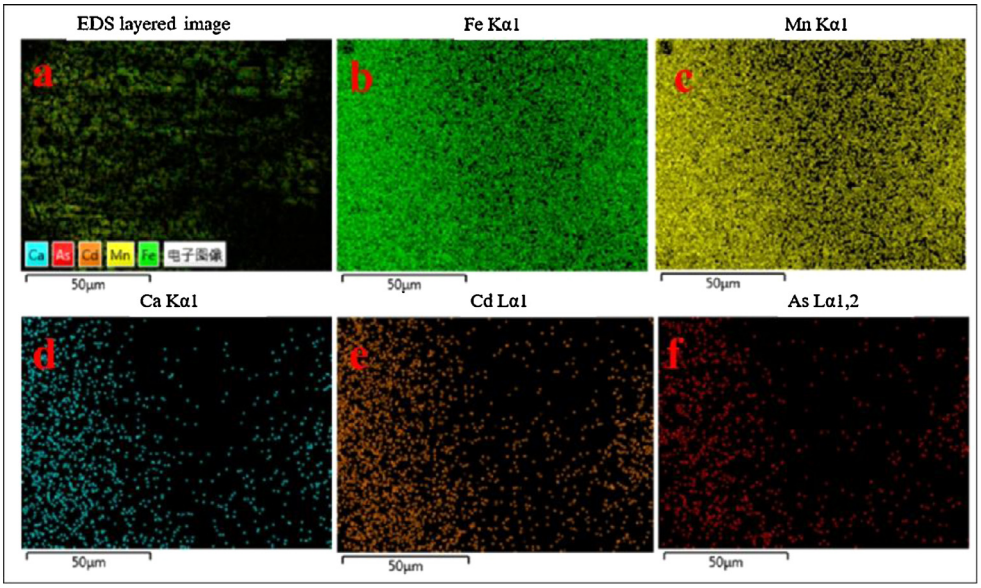

Fig. 7 – Elemental mapping images of 1%Ca-SFMBO after As-Cd adsorption. (a) EDS layered image; (b) Fe; (c) Mn; (d) Ca; (e) Cd; (f) As. The initial As(III) concentration of 30 mg/L and initial Cd(II) concentration of 30 mg/L with equilibrium time of 24 hr. for As(III) and Cd(II).

sorbents (Gallios et al., 2017; Lou et al., 2017). In the process of heavy metal adsorption (Fig. 5b), MnO_2 (centered at 642.4 eV and 654.1 eV) in SFMBO and Ca-SFMBO was transformed into MnOOH (centered at 641.7 eV and 653.4 eV) and MnO (centered at 640.7 eV and 652.4 eV), which was reflected in the decrease in peak areas of the former and the appearance of compound peaks of the latter (Ocinski et al., 2016; Xu et al., 2019). However, according to calculated peak areas, the oxidation efficiency of MnO_2 in SFMBO was not the same as that in Ca-SFMBO. After As-Cd adsorption, the contents of MnO_2, MnOOH and MnO in SFMBO were 20.21%, 68.54% and 21.25%, respectively, and the corresponding values for Ca-SFMBO were 24.96%, 57.54% and 17.50%. This was because the adsorption sites of Cd(II) increased after the surface calcification treatment to give Ca-SFMBO, and the adsorption of Cd(II) prevented contact between As(III) and MnO_2, reducing the oxidation rate of MnO_2 (Wu et al., 2018).

Peaks corresponding to As(V) (centered at 46.2 eV) and Cd(II) (centered at 405.1 eV) are shown in Fig. 5c, and d. There was no difference between the two adsorbents, where As(III) was basically oxidized to As(V), indicating similar adsorption products.

Fig. 6 shows the FT-IR spectra of SFMBO and Ca-SFMBO particles before and after As-Cd adsorption. The peaks around 1630 cm^{-1} and 3363 cm^{-1} were associated with the elastic vibration of hydroxyl groups (Gupta et al., 2012). The peaks of Ca-SFMBO (3355 cm^{-1} and 3380 cm^{-1}) were shifted to higher wavenumbers when compared with the peaks of SFMBO (3375 cm^{-1} and 3351 cm^{-1}). This was because in $CaCO_3$-modified SFMBO, Ca ions bonded to the material surface, which changed the surface chemistry of the material and was reflected in changes to the hydroxyl groups. The peaks at 1122 cm^{-1} and about 530 cm^{-1} were respectively due to the C-O bond elastic vibration and the presence of inorganic ions (Zhang et al., 2009a). The peaks due to inorganic ions showed slight shifts after material adsorption, such as 534 cm^{-1} to 520 cm^{-1} for SFMBO and 541 cm^{-1} to 511 cm^{-1} for Ca-SFMBO. This was because the surface chemistry around the inorganic ions Fe and Mn changed during the adsorption process, leading to shifts in the inorganic peak positions. After heavy metal adsorption, both SFMBO and Ca-SFMBO generated new peaks at 1384 cm^{-1}, which was attributed to the production of a new ternary Fe-As-Cd inorganic complex.

Fig. 7 shows elemental mapping images of Ca-SFMBO after As-Cd adsorption. It can be seen that the distributions of Fe and Mn were relatively uniform (Fig. 7b, and c). However, it should be noted that dissolution of Fe and Mn from the material will occur during the treatment of metals in water by iron/manganese materials (Ryu et al., 2017, Sun et al., 2018). This might affect the adsorption capacities of the materials, and needs more study. The distributions of Ca, As and Cd were similar (Fig. 7d–f). It was speculated that the Fe-As-Cd ternary complex was formed as follows: As(III) was oxidized and adsorbed, and then Cd(II) was adsorbed again at the same position. The adsorbed content of Cd(II) was higher than that of As(III), which was because of the relatively high concentration of Cd(II) (30 mg/L) in solution. Cd(II) may compete with As(III) for adsorption sites on the surface of Ca-SFMBO and inhibit the adsorption of As(III). Moreover, Cd(II) could also be adsorbed at sites where As(III) ions are adsorbed due to chemical complexation.

3. Conclusion

A Ca-SFMBO adsorbent was prepared through co-precipitation with a novel Fe/Mn ratio, synthetic pH, stabilizer (starch) and surface modifier. It could be seen from XRD and SEM results that Ca-SFMBO consists of amorphous oxide particles. In the optimal adsorption pH experiment, Ca-SFMBO could stabilize the pH in solution over a wide range. In single-adsorption systems, the optimal pH and mechanism of As(III) and Cd(II) adsorption were different, and the optimal pH of As(III)-Cd(II) co-adsorption was 6. In the dual-adsorbate system, the presence of Cd(II) at low concentrations enhanced As(III) adsorption by 33.3%, while the adsorption of As(III) was inhibited with increasing Cd(II) concentration. The possible adsorption mechanisms were inferred as electrostatic physical adsorption, chemical adsorption and chemical complexation adsorption. A new stable chemical bond was formed between As and

Cd on Ca-SFMBO, forming a ternary complex. Based on XPS analysis, the hydroxyl of Mn was closely related to the oxidation of As(III) and the hydroxyl of Fe was related to the adsorption of As and Cd. However, the addition of $CaCO_3$ destroyed the acid-base balance in the synthesis process of SFMBO, resulting in irregular Ca-SFMBO particles, and reduced the oxidation efficiency of Mn(IV). FTIR and EDS analysis speculated the formation of a ternary Fe-As-Cd complex. In conclusion, the developed Ca-SFMBO adsorbent shows promise for application in the treatment of arsenic- and cadmium-contaminated water.

Acknowledgments

This work was supported by the National Key Technology R&D Program (No. 2018YFD0800202).

REFERENCES

Agrafioti, E., Kalderis, D., Diamadopoulos, E., 2014. Arsenic and chromium removal from water using biochars derived from rice husk, organic solid wastes and sewage sludge. J.Environ.Manag. 133, 309–314.

Barrett, J.R., 2012. A potential window onto early pancreatic cancer development evidence of cancer stem cell growth after exposure to cadmium chloride in vitro. Environ. Health Perspect. 120 A363-A363.

Cao, C.Y., Qu, J., Yan, W.S., Zhu, J.F., Wu, Z.Y., Song, W.G., 2012. Low-cost synthesis of flowerlike alpha-Fe_2O_3 nanostructures for heavy metal ion removal: adsorption property and mechanism. Langmuir 28, 4573–4579.

Chun, Y., Shu, Q.H., He, Y.G., 2004. Study on acid modification of the outer surface of HZSM-5 zeolite by calcium carbonate. Petrochem. Technol. 33, 1134–1135.

De Gisi, S., Lofrano, G., Grassi, M., Notarnicola, M., 2016. Characteristics and adsorption capacities of low-cost sorbents for wastewater treatment: a review. Sustain. Mater. Technol. 9, 10–40.

Deng, J.H., Zhang, X.R., Zeng, G.M., Gong, J.L., Niu, Q.Y., Liang, J., 2013. Simultaneous removal of Cd(II) and ionic dyes from aqueous solution using magnetic graphene oxide nanocomposite as an adsorbent. Chem. Eng. J. 226, 189–200.

Ebinger, M.H., Schulze, D.G., 1990. The influence of pH of the synthesis of mixed Fe-Mn oxide minerals. Clay Min 25, 507–518.

Fisher, A.T., Lopez-Carrillo, L., Gamboa-Loira, B., Cebrian, M.E., 2017. Standards for arsenic in drinking water: Implications for policy in Mexico. J. Public Health Pol. 38, 395–406.

Gallios, G.P., Tolkou, A.K., Katsoyiannis, I.A., Stefusova, K., Vaclavikova, M., Deliyanni, E.A., 2017. Adsorption of arsenate by nano scaled activated carbon modified by iron and manganese oxides. Sustainability 9, 18.

Gu, C.P., Guan, W.M., Shim, J.J., Fang, Z., Huang, J.R., 2017. Size-controlled synthesis and electrochemical performance of porous Fe_2O_3/SnO_2 nanocubes as an anode material for lithium ion batteries. Crystengcomm 19, 708–715.

Guan, C., Liu, L., Liu, Y.J., Li, R.D., 2017. Effictiveness of acid-dye waste water treated by $CaCO_3$ modified diatomite. Sci. Tech. Engrg. 23, 333–336.

Gupta, V.K., Nayak, A., Agarwal, S., Dobhal, R., Uniyal, D.P., Singh, P., et al., 2012. . Arsenic speciation analysis and remediation techniques in drinking water. Desalin. Water Treat. 40, 231–243.

Gurgel, L.V., Junior, O.K., Gil, R.P., Gil, L.F., 2008. Adsorption of Cu(II), Cd(II), and Pb(II) from aqueous single metal solutions by cellulose and mercerized cellulose chemically modified with succinic anhydride. Bioresour. Technol. 99, 3077–3083.

Han, X., Liang, C.F., Li, T.Q., Wang, K., Huang, H.G., Yang, X.E., 2013. Simultaneous removal of cadmium and sulfamethoxazole from aqueous solution by rice straw biochar. J. Zhejiang Univ.-SCI. B 14, 640–649.

Han, Z.T., Sani, B., Mrozik, W., Obst, M., Beckingham, B., Karapanagioti, H.K., et al., 2015. . Magnetite impregnation effects on the sorbent properties of activated carbons and biochars. Water Res. 70, 394–403.

Hu, S., Yan, L., Chan, T., Jing, C., 2015. Molecular insights into ternary surface complexation of arsenite and cadmium on TiO_2. Environ. Sci. Technol. 49, 5973–5979.

Kyzas, G.Z., Matis, K.A., 2015. Nanoadsorbents for pollutants removal: a review. J. Mol. Liq. 203, 159–168.

Lin, L.N., Qiu, W.W., Wang, D., Huang, Q., Song, Z.G., Chau, H.W., 2017. Arsenic removal in aqueous solution by a novel Fe-Mn modified biochar composite: Characterization and mechanism. Ecotox. Environ. Safe. 144, 514–521.

Liu, R.P., Liu, F., Hu, C.Z., He, Z., Liu, H.J., Qu, J.H., 2015. Simultaneous removal of Cd(II) and Sb(V) by Fe-Mn binary oxide: positive effects of Cd(II) on Sb(V) adsorption. J. Hazard. Mater. 300, 847–854.

Lou, Z.M., Cao, Z., Xu, J., Zhou, X.X., Zhu, J., Liu, X., Baig, S.A., et al., 2017. . Enhanced removal of As(III)/(V) from water by simultaneously supported and stabilized Fe-Mn binary oxide nanohybrids. Chem. Eng. J. 322, 710–721.

Lubin, J.H., Moore, L.E., Fraumeni, J.F., Cantor, K.A., 2008. Respiratory cancer and inhaled inorganic arsenic in copper smelters workers: a linear relationship with cumulative exposure that increases with concentration. Environ. Health Perspect. 116, 1661–1665.

Ma, W., Song, X.Y., Pan, Y.Q., Cheng, Z.H., Xin, G., Wang, B.D., et al., 2012. . Adsorption behavior of crystal violet onto opal and reuse feasibility of opal-dye sludge for binding heavy metals from aqueous solutions. Chem. Eng. J. 193, 381–390.

McCann, C.M., Peacock, C.L., Hudson-EdWards, K.A., Shrimpton, T., Gray, N.D., Johnson, K.L., 2018. In situ arsenic oxidation and sorption by a Fe-Mn binary oxide waste in soil. J. Hazard. Mater. 342, 724–731.

Mishra, A.K., Ramaprabhu, S., 2010. Magnetite decorated multiwalled carbon nanotube based supercapacitor for arsenic removal and desalination of seawater. J. Phys. Chem. C 114, 2583–2590.

Ocinski, D., Jacukowicz-Sobala, I., Mazur, P., Raczyk, J., Kociolek-Balawejder, E., 2016. Water treatment residuals containing iron and manganese oxides for arsenic removal from water - characterization of physicochemical properties and adsorption studies. Chem. Eng. J. 294, 210–221.

Pandey, P.K., Choubey, S., Verma, Y., Pandey, M., Chandrashekhar, K., 2009. Biosorptive removal of arsenic from drinking water. Bioresource. Technol. 100, 634–637.

Reddy, D.H.K., Lee, S.M., 2014. Magnetic biochar composite: Facile synthesis, characterization, and application for heavy metal removal. Colloid Surf. -Physicochem. Eng. Asp. 454, 96–103.

Roonasi, P., Holmgren, A., 2009. A Fourier transform infrared (FTIR) and thermogravimetric analysis (TGA) study of oleate adsorbed on magnetite nano-particle surface. Appl. Surf. Sci. 255, 5891–5895.

Ryu, S.R., Jeon, E.K., Yang, J.S., Baek, K., 2017. Adsorption of As(III) and As(V) in groundwater by Fe-Mn binary oxide-impregnated granular activated carbon (IMIGAC). J. Taiwan Inst. Chem. Eng. 72, 62–69.

Shan, C., Tong, M.P., 2013. Efficient removal of trace arsenite through oxidation and adsorption by magnetic nanoparticles modified with Fe-Mn binary oxide. Water Res. 47, 3411–3421.

Sheng, P.X., Ting, Y.P., Chen, J.P., Hong, L., 2004. Sorption of lead, copper, cadmium, zinc, and nickel by marine algal biomass: characterization of biosorptive capacity and investigation of mechanisms. J. Colloid Interface Sci. 275, 131–141.

Sullivan, C., Tyrer, M., Cheeseman, C.R., Graham, N.J.D., 2010. Disposal of water treatment wastes containing arsenic - a review. Sci. Total Environ. 408, 1770–1778.

Sun, Y., Liu, Y.L., Lou, Z.M., Yang, K.L., Lv, D., Zhou, J.S., et al., 2018. Enhanced performance for Hg(II) removal using biomaterial (CMC/gelatin/starch) stabilized FeS nanoparticles: Stabilization effects and removal mechanism. Chem. Eng. J. 344, 616–624.

Ungureanu, G., Santos, S., Boaventura, R., Botelho, C., 2015. Arsenic and antimony in water and wastewater: overview of removal techniques with special reference to latest advances in adsorption. J. Environ. Manag. 151, 326–342.

Wang, K.J., Xing, B.S., 2004. Mutual effects of cadmium and phosphate on their adsorption and desorption by goethite. Environ. Pollut. 127, 13–20.

Wu, J.Z., Huang, D., Liu, X.M., Meng, J., Tang, C.X., Xu, J.M., 2018. Remediation of As(III) and Cd(II) co-contamination and its mechanism in aqueous systems by a novel calcium-based magnetic biochar. J. Hazard. Mater. 348, 10–19.

Wu, Y., Li, W., Sparks, D.L., 2015. The effects of iron(II) on the kinetics of arsenic oxidation and sorption on manganese oxides. J. Colloid Interface Sci. 457, 319–328.

Xiong, Y., Tong, Q., Shan, W.J., Xing, Z.Q., Wang, Y.J., Wen, S.Q., et al., 2017. Arsenic transformation and adsorption by iron hydroxide/manganese dioxide doped straw activated carbon. Appl. Surf. Sci. 416, 618–627.

Xu, F.N., Chen, H.X., Dai, Y.X., Wu, S.L., Tang, X.J., 2019. Arsenic adsorption and removal by a new starch stabilized ferromanganese binary oxide in water. J. Environ. Manag. 245, 160–167.

Yang, K., Zhu, L.Z., Xing, B.S., 2006. Adsorption of polycyclic aromatic hydrocarbons by carbon nanomaterials. Environ. Sci. Technol 40, 1855–1861.

Xu, W., Lan, H., Wang, H., Liu, H., Qu, J., 2014. Comparing the adsorption behaviors of Cd, Cu and Pb from water onto Fe-Mn binary oxide, MnO_2 and FeOOH. Front Environ. Sci. Engl. 9.

Yan, L., Huang, Y.Y., Cui, J.L., Jing, C.Y., 2015. Simultaneous As(III) and Cd removal from copper smelting wastewater using granular TiO_2 columns. Water Res 68, 572–579.

Yang, W.C., Kan, A.T., Chen, W., Tomson, M.B., 2010. pH-dependent effect of zinc on arsenic adsorption to magnetite nanoparticles. Water Res. 44, 5693–5701.

Zhang, G.S., Liu, H.J., Liu, R.P., Qu, J.H., 2009a. Adsorption behavior and mechanism of arsenate at Fe-Mn binary oxide/water interface. J. Hazard. Mater. 168, 820–825.

Zhang, G.S., Liu, H.J., Liu, R.P., Qu, J.H., 2009b. Removal of phosphate from water by a Fe-Mn binary oxide adsorbent. J. Colloid Interface Sci. 335, 168–174.

Zhang, S.X., Niu, H.Y., Cai, Y.Q., Zhao, X.L., Shi, Y.L., 2010. Arsenite and arsenate adsorption on coprecipitated bimetal oxide magnetic nanomaterials: $MnFe_2O_4$ and $CoFe_2O_4$. Chem. Eng. J. 158, 599–607.

Zhao, K.L., Fu, W.J., Qiu, Q.Z., Ye, Z.Q., Li, Y.F., Tunney, H., et al., 2019. Spatial patterns of potentially hazardous metals in paddy soils in a typical electrical waste dismantling area and their pollution characteristics. Geoderma 337, 453–462.